AIAA SciTech Forum
11–15 & 19–21 January 2021, VIRTUAL EVENT
AIAA Scitech 2021 Forum

10.2514/6.2021-0552

High Resolution Modeling for Deeper Understanding of Plasma Dynamics

Toyofumi Yamauchi*, Nakul Nuwal†, Animesh Sharma‡,
Deborah A. Levin§, and Joshua L. Rovey¶

I. Introduction

The Air Force Research Laboratory (AFRL) has been and continues developing and advancing models to predict and understand the behavior of plasma electric propulsion systems, such as Hall effect thrusters (HETs) and field-reversed configurations (FRCs). The fundamental work proposed here supports both operational systems, i.e. HETs, and R&D for next generational plasma propulsion capabilities, i.e. FRCs. These plasma electric propulsion systems are dynamic systems with temporal changes and oscillations in the plasma conditions (e.g., breathing mode (10's kHz) or pulsed inductive fields (100's kHz)), and these dynamic plasma changes give rise to dynamic system operation (fluctuations in performance). Previous models have been developed to predict the *quasi-steady* plasma conditions and performance of these systems (e.g., quasi-steady density, temperature, ion energy in HET channel/plume, quasi-steady thrust/specific impulse). These codes also use approximate electron transport models for some of the thrusters and other plasma physics applications. These previous models are benchmarked and validated with quasi-steady experimental measurements. Further, the model validation data are rarely the raw experimental measurements. Instead, the raw experimental data are analyzed using probe theory,[1] which inherently has assumptions such as Maxwellian particle distribution. Because of these approximate models and experimental data analyses, the major problem is that these previous models and experiments do not capture the true system state. They approximate, ignore, or assume important dynamics and characteristics of the system. New models are now being developed with shorter timescales that can better capture the dynamics of these systems (i.e. the fast temporal fluctuations/changes inherent to these systems), and eliminate the need for approximate models and assumed system characteristics. Models being developed at the AFRL and in academia (e.g., our in-house CHAOS code[2]) can

*Graduate Student, Department of Aerospace Engineering, University of Illinois, Urbana-Champaign, IL 61801.
†Graduate Student, Department of Aerospace Engineering, University of Illinois, Urbana-Champaign, IL 61801.
‡Postdoctoral Researcher, Department of Aerospace Engineering, University of Illinois, Urbana-Champaign, IL 61801.
§Professor, Department of Aerospace Engineering, University of Illinois, Urbana-Champaign, IL 61801.
¶Associate Professor, Department of Aerospace Engineering, University of Illinois, Urbana-Champaign, IL 61801.

predict the temporal evolution of the plasma and performance of these systems, eliminating the need for approximate models by directly simulating the physics on very short timescales (i.e. electron timescale). But an important question still exists: Can we use these new models to aid our understanding of the true dynamics and characteristics of the plasma system? Hence, this work focuses on high temporal resolution kinetic physics-based models validated with raw experimental data, and thereby demonstrates a new approach to model validation that promises to provide a deeper understanding of plasma propulsion system dynamics.

II. Numerical Modeling

The numerical study is conducted on a setup where a flat-plate conductor is embedded in a quasi-neutral plasma, and a nano-second time-scale pulse of electric potential is applied to the conductor. The distance between the pulsed plate and collector plate is 100 mm in a numerical domain of size $10 \times 100 \times 100$ mm, as shown in Fig. 2(a). The size of this domain is about 20 Debye lengths and is sufficient to capture the electron plasma sheath formed when a potential of -100 V is applied to the pulse plate.[3] High-fidelity kinetic Particle-In-Cell (PIC) model with time-explicit scheme is used to perform time-accurate calculations. Our in-house hybrid CPU-GPU based code CHAOS,[4] which is used for the task, solves Poisson's equation for calculating the quasi-steady electric field and then moves the charged particles to resolve the plasma kinetics. The effects of magnetic field effects by the multi-poles of the experimental chamber is ignored since the magnetic field intensity near the computational domain is very low ($< 10^{-6}$ Tesla). The domain is initialized with a plasma density of 1×10^{13} m^{-3} and $T_e = 6$ eV based on the experimental conditions in Langendorf et al.[5] Depending on the number of species present, a proportional number of computational particles are assigned random locations in the domain.

A. Validation of the code : Steady planer sheath near biased plate

As a precursor to the temporal pulsed-plasma study, we performed a numerical calculation on a numerical domain, shown in Fig. 1(a) with a constant bias potential of -100 V applied to the pulse plate. About 900,000 charged particles of each species were used for this calculation and the plasma sheath, shown in Fig. 1(b), reached steady state in 200,000 time-steps (4 μs). Figure 1(b) shows a comparison between plasma sheath profiles based on the number density criteria[6] and the Bohm sheath criteria.[7] The profile based on the ratio of number density compares well with Planar sheath model,[8] but underestimates the Bohm sheath criteria which usually only applies to one-dimensional plasma systems.

B. Boundary conditions for homogeneous quasi-neutral plasma

To model the pulsed-plasma in the plasma chamber, we require a homogeneous quasi-neutral Maxwellian plasma as the initial condition before we introduce any temporal variations in the domain. To that effect, the numerical domain is filled with plasma of density $n_e = n_i = 1 \times 10^{13}$ m^{-3}. The charged particles can leave the domain from the conducting plates at $z = 0$ and $z = 100$ mm, and domain boundaries in the y direction. Since in our experiments, the source of the plasma lies outside the numerical domain, we replenish the charged particles by initializing new particles in 5 mm thick regions near $y = 0$ mm and $y = 100$ mm boundaries

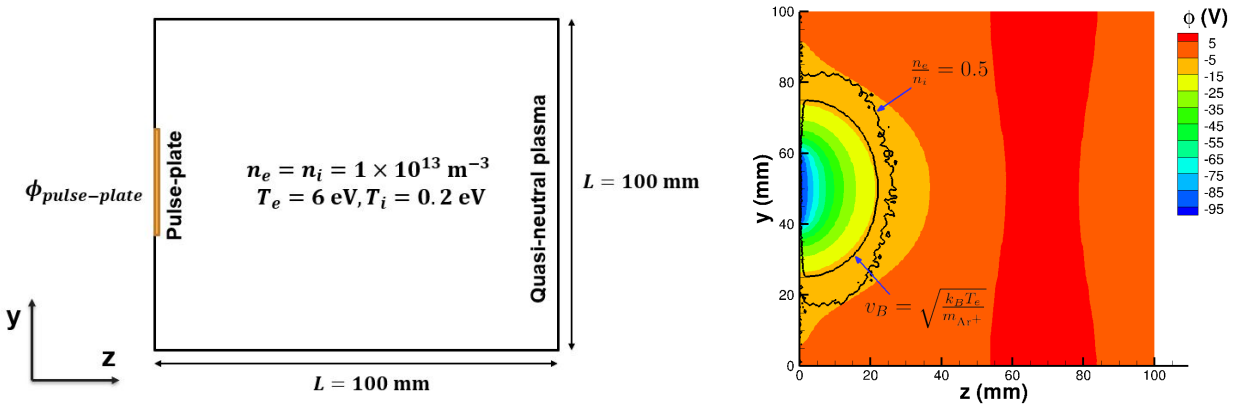

(a) Schematic for the case with a plate with a constant bias potential.

(b) Ion plasma sheath based on different sheath criteria

Figure 1. Comparison of ion plasma sheath profiles near the biased plate based on different sheath criteria. Here, v_B is the Bohm speed of ions and $\phi_{pulse-plate} = -100$ V.

shown by dashed lines in Fig. 2(a). This boundary towards the domain edges in y direction maintains the total charge in the domain without interfering with the plasma between the pulse-plate and the collector plate. The charged particles are specularly reflected from non-conductive regions of $z = 0$ and $z = 100$ mm boundaries as shown in Fig. 2(a) to represent the symmetry of plasma on either sides of z direction domain edges. These boundary conditions result in a Maxwellian particle z-velocity distribution, as shown in Fig. 2(b), at steady state.

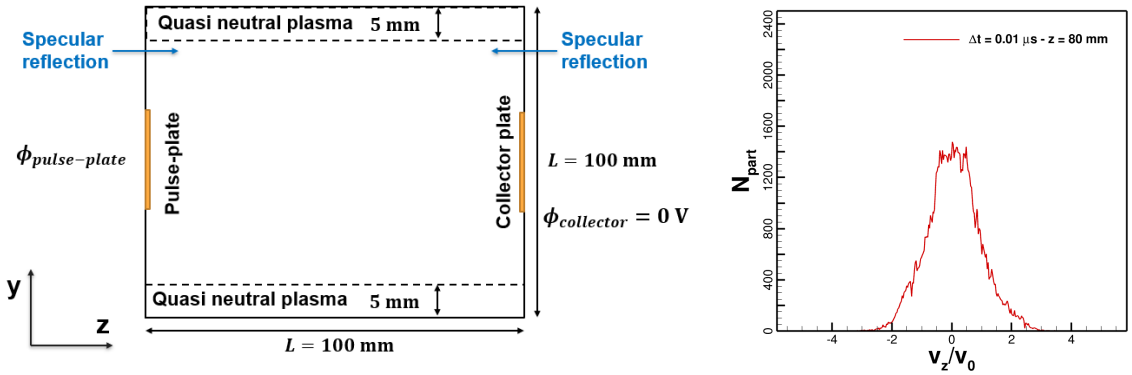

(a) Schematic of the test box.

(b) EV_zDF in the plasma without pulse.

Figure 2. Schematic of the test box. The plate on the left side is the pulse-plate, and on the right is the collector plate. The z-velocity distribution is nearly a Maxwellian before at the beginning of the pulse.

C. Temporal variation of plasma with a 0.2 μs pulse

Once a steady Maxwellian plasma formed in the center of the domain, a linear plasma pulse[9] of 0.2 μs rise-time is applied on the pulse-plate shown in Fig. 2(a) while maintaining

the collector plate at 0 V. A time-varying potential at pulse plate is applied using a Dirichlet boundary condition,

$$\phi_{\text{pulse-plate}}(t) = \begin{cases} 0 \text{ V} & \text{if } \Delta t < 0, \\ -100\frac{(t-t_{\text{start}})}{t_{\text{pulse}}} \text{ V} & \text{if } 0 < \Delta t < t_{\text{pulse}}, \\ -100 \text{ V} & \text{if } t_{\text{pulse}} < \Delta t, \end{cases} \tag{1}$$

where $\Delta t = t - t_{\text{start}}$, and t_{pulse} is the rise-time of the pulse. For this subsection, $t_{\text{start}} = 0.2\ \mu s$ and $t_{\text{pulse}} = 0.2\ \mu s$. The electrons near the pulse plate are repelled by the negative potential of the plate as the pulse is applied and an ion plasma sheath forms and expands with time.

Based on the steady state calculations, shown in Fig. 1, the sheath edge for -100 V bias lies near $z = 20$ mm. As the pulse progresses in time, the electric potential at $(y, z) = (50, 20)$ mm drops and oscillates with a timescale $\tau = 0.07\ \mu s$, as shown in Fig. 3(a). The electric potential at the other probe locations also oscillates but for probes at $z > 20$ mm, as shown in Fig. 3(a), it does not trend towards a more negative value. The oscillatory behavior of electrons is also seen in the collected current at the collector as shown in Fig. 3(b). This shows that the electric potential in plasma, and the collector current are in direct co-relation with each other. The oscillatory behavior of the electrons will be discussed further in the following section.

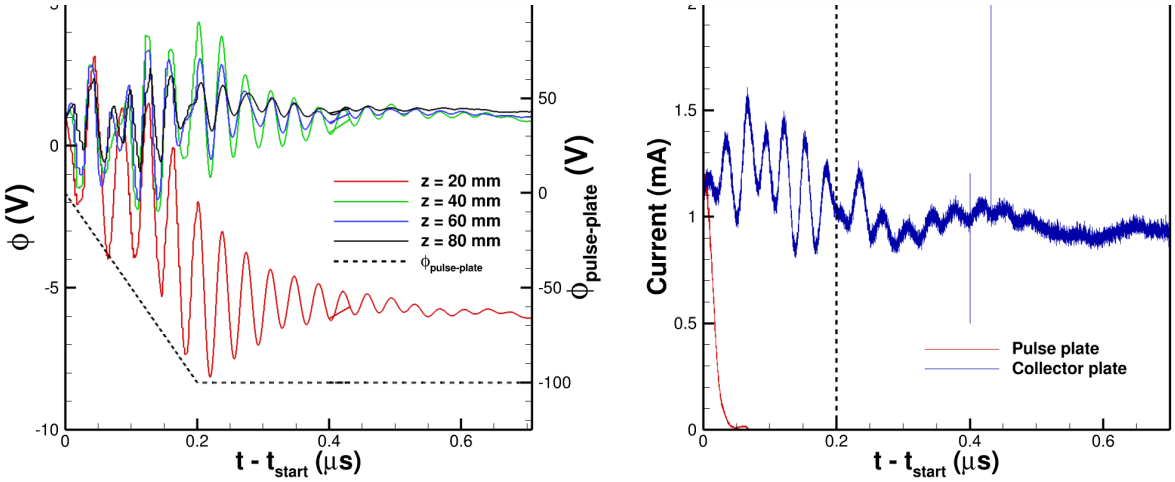

(a) Electric potential with time at different probe locations.

(b) Electron current at pulse plate and collector plate. Dashed line indicates the end of the linear pulse.

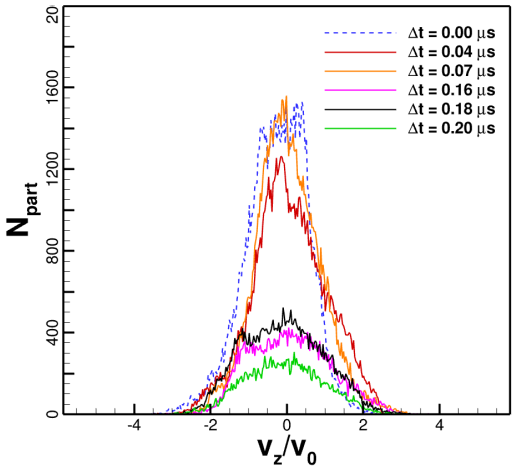

(c) EV_zDF at $y = 50$ mm, $z = 20$ mm

Figure 3. Temporal variation of plasma parameters for a pulse of 0.2 μs**.**

D. Mechanism of oscillations for a 0.2 μs plasma pulse

The time-scale of the oscillations, $\tau = 0.07$ μs, which is closer to the electron plasma frequency, indicates that the electrons' response to the pulse is responsible for the oscillations in the plasma. For every bias potential of the pulse plate, there is a corresponding steady state plasma sheath which would form if the system was left to evolve with a constant value of $\phi_{\text{pulse}-\text{plate}}$. However, when $\phi_{\text{pulse}-\text{plate}}(t)$ changes in a short time, the plasma sheath expands rapidly, and the electrons, especially near the plasma sheath edge, oscillate about their 'steady state' position. This oscillatory behavior is also evident in the z-velocity distribution function for electrons at $z = 20$ mm as shown in Fig. 3(c) where the peak is shown to oscillate between $\Delta t = 0.0, 0.04,$ and 0.07 μs and then again between $\Delta t = 0.16, 0.18,$ and 0.20 μs. Also, the declining EV_zDF peak in Fig. 3(c) shows that the electrons are leaving the expanding plasma sheath. The EV_zDF's are relatively less affected at the locations $z > 20$ mm, i.e. the region outside the ion plasma sheath. The mechanism of these waves will be studied in future work.

III. Experiments

The objective of the experiments in this work is to validate the kinetic numerical model and extract raw plasma dynamics data for high-frequency variations in plasma. The following sections describe the experimental facility and the preliminary diagnostics performed on the low-density plasma.

A. Vacuum Facility

All experiments are conducted at the University of Illinois at Urbana-Champaign in the Electric Propulsion Laboratory vacuum chamber, which is 1.2 m diameter and 2.1 m long. The chamber is evacuated to 10 mTorr (133 mPa) rough vacuum by a Kinney KT150 rotary piston pump in line with an NRC and roots blower mechanical pumps. High vacuum is achieved with 1.2-m diameter TM1200 cryopump and the chamber base pressure is typically 5×10^{-8} Torr. An Alicat MCV (MCV-500SCCM-D-DB15-PCV10) mass flow controller is used to control the flow of Argon gas into the chamber and all experiments used a flow rate of 300 sccm. The pressure is measured by measured by KJLC Cold Cathode Pirani Gauge (KJLC CCPG-H2-6) and at the prescribed flow rate the equilibrium chamber pressure is $7.5 \pm 1.5 \times 10^{-5}$ Torr for all experiments. The ion-neutral mean-free-path corresponding to the experimental pressure is 0.8 ± 0.1 m.

B. Multipole Plasma Cell

Plasma is generated in a multipole plasma cell (MPC). Multipole plasma cells have been extensively used for plasma sheath studies and ion acoustic wave studies by other researchers.[10,11] The MPC used in the experiments here is shown in Figure 4. The MPC is cylindrical with 20 inch diameter and 32 inch long and made of 24 aluminum u-channels holding nine CM-0127 ceramic disk magnets in line. The magnets are oriented with the same polarity on each u-channel with adjacent u-channels assigned opposing polarities to configure a broken line cusp magnetic field.[12] The magnets are equally spaced 2 inch apart on center along the u-channels. A schematic of the electrical setup is shown in Figure 5. The MPC is electrically grounded to the vacuum chamber. Electrons are emitted thermionically into the MPC by an array of five 0.005 inch diameter tungsten filaments heated by electrical current supplied with a TDK-Lambda GENH30V-25A DC power supply. The filaments are placed along the x-axis. The plasma discharge is formed by negatively biasing the filaments with respect to the MPC (i.e., ground) with a Kepco BOP 1000M power supply. The nominal filament heating current is 7.0 A for a 10 mA discharge current.

C. Probe Diagnostic

Inside the MPC, the are two square electrodes having aside of 20 mm made of a stainless steel, separated by 100 mm and parallel to each other. One electrode is a "pulser" that will be connected to the pulse generating circuit to perturb the plasma with a hundred of microsecond pulse. Another electrode is a "collector" that will measure the change in current due to the perturbation. Both electrodes are parallelly placed in x-y plane. The steady-state plasma properties are measured by the electrostatic probes. Both electrostatic probes are positioned at the middle of two electrodes by Velmex XSlide linear motion stages. The Langmuir probe

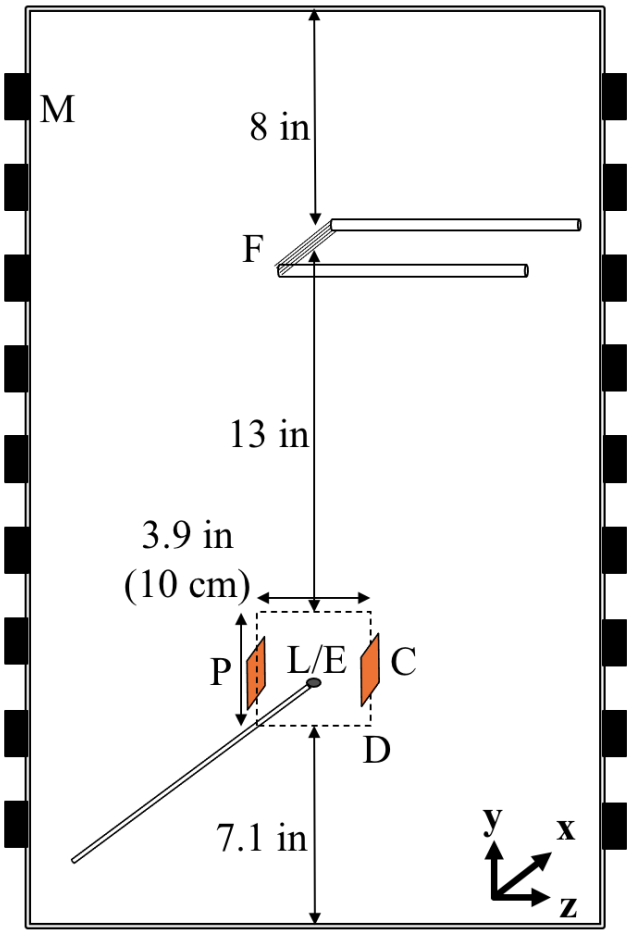

Figure 4. Experimental Setup; M = magnets, F = filaments, P = pulser electrode, C = collector electrode, D = computational domain, L/E = Langmuir/emissive probe

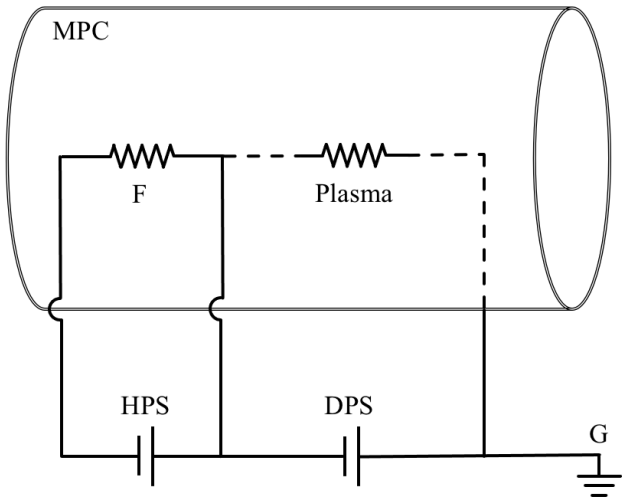

Figure 5. Electrical setup; MPC = multipole plasma cell, F = filament, HPS = heating power supply, DPS = discharge power supply, G = ground (vacuum chamber)

is oriented so that its flat surface is facing to the filaments (the flat surface is on x-z plane). The filament array, the electrostatic probes, and the electrodes are positioned along the center of the cylinder in order to minimize the magnetic field strength of the MPC.

The plasma potential is measured by an emissive probe. The emissive probe is a "hair-pin" design that is made of ceramic tubing of 0.188 inch diameter with tungsten wire tip of 0.005 inch diameter. The emissive probe is heated by Sorensen DLM 20V-30A DC power supply and biased by Keithley 2410 Sourcemeter. Keithley 2410 Sourcemeter also measures the current through the emissive probe. Nominal heating power is 3.5 V and 2.4 A. The measured plasma potential is -14 ± 2.5 V for all test conditions.

Bulk plasma properties are measured by a Langmuir probe. The Langmuir probe is a planar, disk-shaped and made of ceramic tubing of 0.188 inch diameter with tungsten tip of 0.77 mm diameter and 0.5 mm thickness. The planer shape is selected to increase the collecting current at the probe and to reduce the error in collected current in the low-density plasma. The collected current is composed of several components. Some of the electrons from the filament do not collide with neutrals before reaching the Langmuir probe and still possess high energy when collected. We call these electrons as primary beam electrons. Some of these primary electrons bounce of the magnetic field of the MPC and lose their unidirectionality. We call these primary electrons as primary isotropic electrons. It is assumed that electrons colliding with neutrals reach to the equilibrium condition and their energy distribution is Maxwellian. Ions are generated by the collisions between neutrals and high energy primary electrons. In summary, the collected probe current is composed of four different sources: ion, primary beam electron, primary isotropic electron, and Maxwellian electrons (Eq. 2).

$$I_{probe} = I_{ion} + I_{pri,beam} + I_{pri,iso} + I_e \tag{2}$$

The I-V curve generated from the Langmuir probe measurements is interpreted as follows. An ion number density (n_i) is determined by fitting the ion current only region with the ion current for the OML theory for spherical probe[13] (Eq.3).

$$I_{ion} = A_p n_i e \sqrt{\frac{kT_i}{2\pi m_i}} \left(1 - \frac{e(V_p - V)}{kT_i}\right) \tag{3}$$

where I_{ion} is the ion current, A_p is the probe area, e is the elementary charge, k is the Boltzmann constant, T_i is the ion temperature, m_i is the ion mass, V_p is the plasma potential, and V is the probe biasing voltage (Figure 6). This application of the theory for spherical probe is valid as the sheath size in the low-density plasma is relatively large and collection field of the probe behaves as the that of the spherical probes. It is evident that the ion current collected by the Langmuir probe shows a linear I-V relationship. The I-V curve is linear until about the discharge voltage (i.e., -150 V in Figure 6), which indicates that all electrons are repelled by the probe due to the biasing voltage. The ion temperature is assumed to be at the room temperature of 22 C. The ion current is corrected for a singly charged Argon ion-induced secondary electron emission for tungsten using the data in previous studies.[14,15]

Next, the fitted ion current is subtracted from the probe current and the remaining current is composed of primary beam, primary isotropic, and Maxwellian electrons (Figure 7). The beam electron number density ($n_{pri,beam}$) is determined by the beam current (Eq.4). The beam portion is approximately located at the discharge voltage.

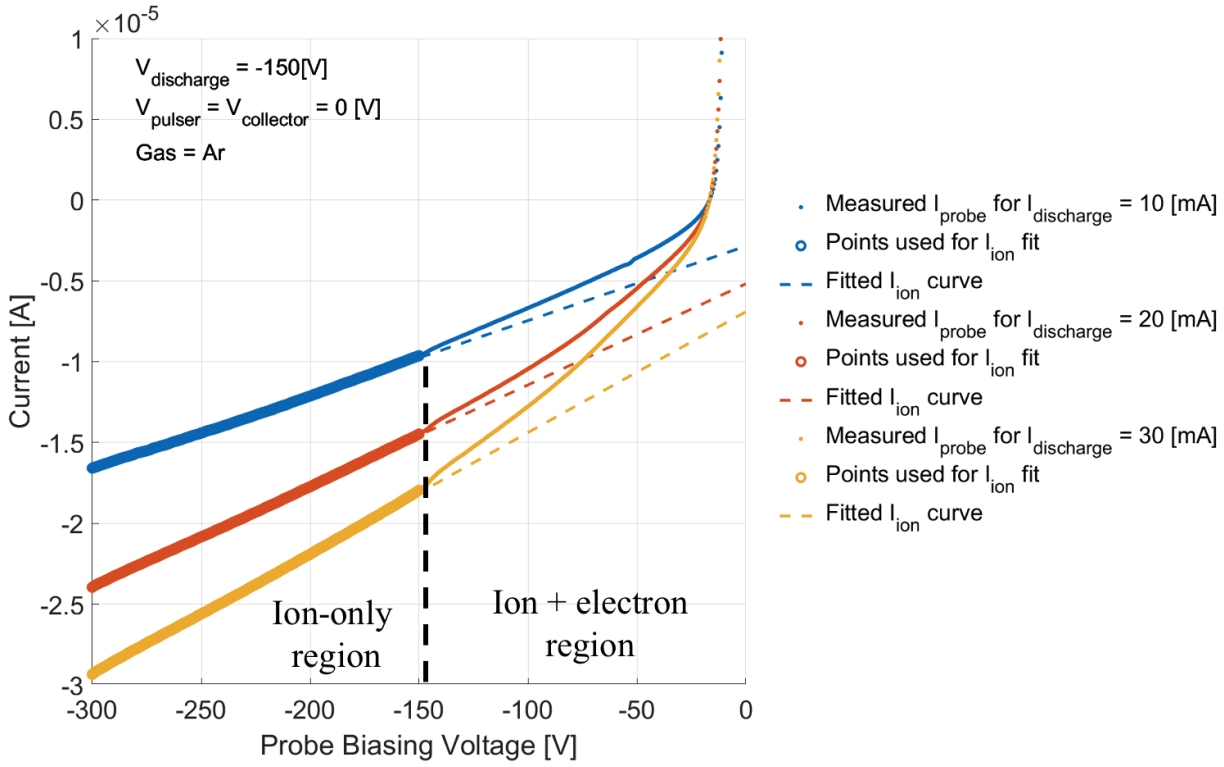

Figure 6. Ion current fit at various discharge currents. The discharge voltage is held at -150 V.

$$I_{pri,beam} = \frac{A_p}{2} n_{pri,beam} e \sqrt{\frac{2(V_{discharge} - V_p)}{m_e}} \tag{4}$$

where $V_{discharge}$ is the discharge voltage (the filament biasing voltage), and m_e is the electron mass. The probe area is halved as the primary beam electrons reach to only one side of the probe. The primary isotropic electron number density ($n_{pri,isotropic}$) is determined by the linear fit (Eq.5).[13]

$$n_{pri,iso} = -\frac{dI}{dV} \frac{2m_e}{e^2 A_p} \sqrt{\frac{2(V_{discharge} - V_p)}{m_e}} \tag{5}$$

where dI/dV is the slope of the primary isotropic portion.

The Maxwellian electron number density is calculated using the quasi-neutral plasma assumption (Eq.6).

$$n_i = n_{pri,iso} + n_{pri,iso} + n_e \tag{6}$$

Finally, the primary electrons are subtracted out as well and the exponential fit is applied for the remaining Maxwellian electron current. The electron temperature is approximated by the exponential fit (Eq.7).

$$I_e \propto \exp\left(\frac{V}{T_e}\right) \tag{7}$$

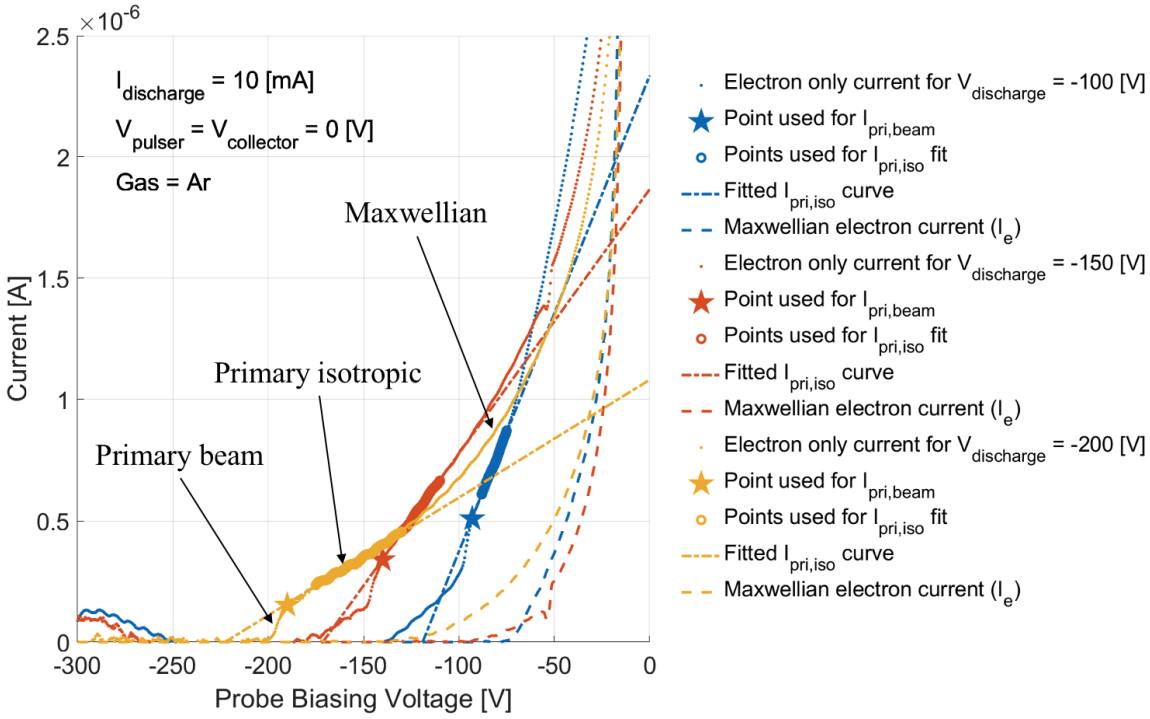

Figure 7. IV curves for primary electrons + Maxwellian electron at various discharge voltage. The beam current is approximately located at the discharge voltage. Dashed lines are the Maxwellian electron IV curves.

D. Steady-state Measurement Results

Figure 8 presents the electron number density as a function of the discharge voltage where the discharge current and the collector biasing voltage are fixed at 10 mA and 0 V (grounded), respectively. The primary beam and isotropic electron densities decreases as the discharge voltage is reduced. This is explained as follows. Decreasing the discharge voltage gives higher energy to the primary electrons. In order to hold the discharge current at constant 10 mA, the number density of the primary electron emitted needs to be lessen because the electrons are emitted with higher velocity at lower discharge voltage. When the pulser electrode is biased at -100 V, the electron number densities decrease. This happens as some of the electrons are repelled out of the measurement domain by the negative potential. The Debye length for the given electron number density is about 1.5 cm. The sheath thickness corresponding to the pulser potential of -100 V is about 23 cm,[3] which is bigger than the electrodes separation distance (i.e., 10 cm). Maxwellian, primary isotropic, and primary beam electron number density increases as the discharge current increases. This occurs because higher discharge current results emission of more electrons and increased interaction with the neutrals.

Figure 9 presents the primary electron energy and electron temperature as a function of the discharge voltage, where the discharge current and the collector biasing voltage are fixed at 10 mA and 0 V (grounded), respectively. The electron temperature remains relatively constant (2-3 eV) with the discharge voltage and pulser biasing voltage. The electron temperature remains same with the discharge current.

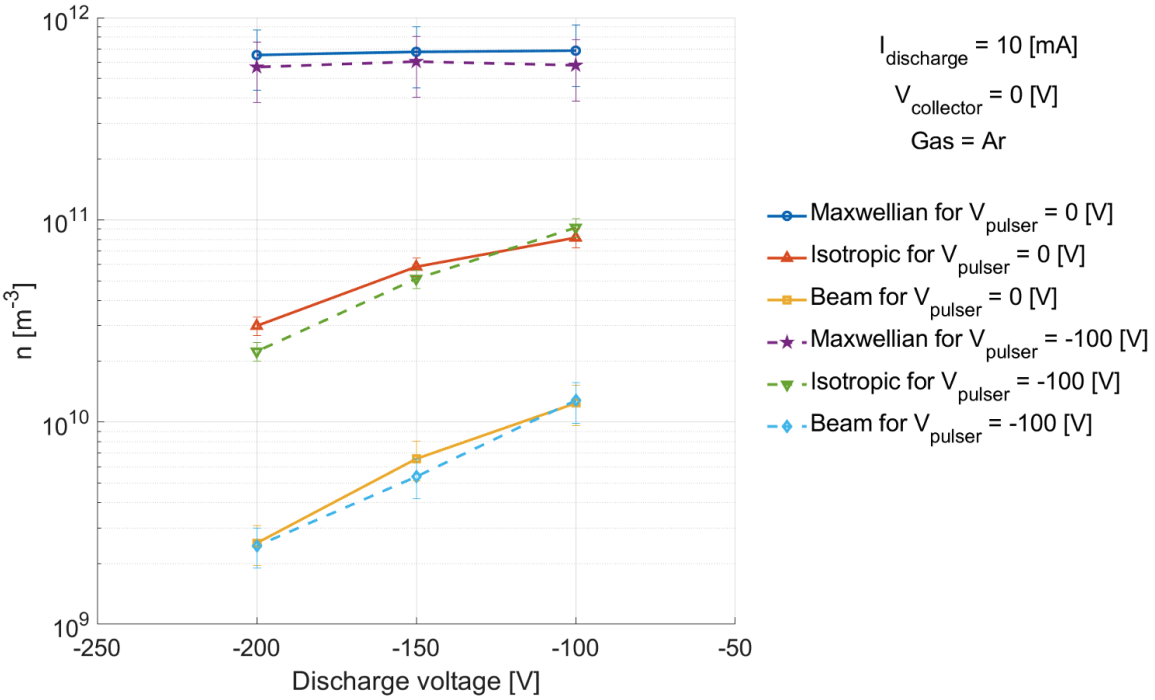

Figure 8. Plasma density vs discharge voltage. The discharge current is held at 10 mA. The collector voltage is held at 0 V. The measurement is taken at the middle between two electrodes.

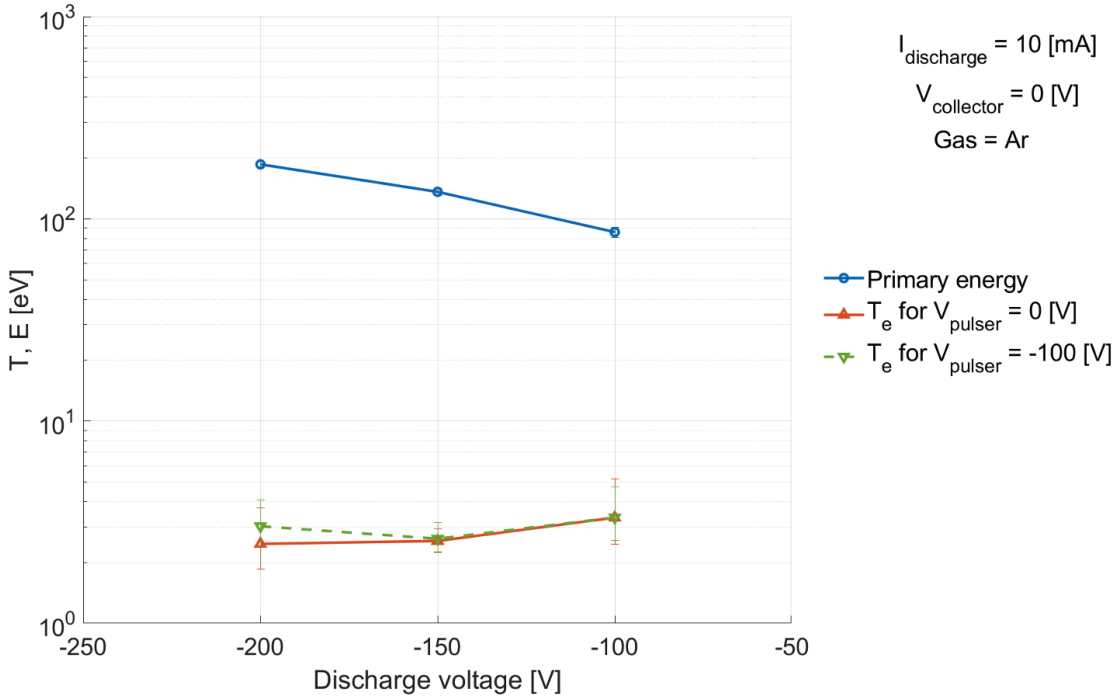

Figure 9. Primary energy and electron temperature vs discharge voltage. The discharge current is held at 10 mA. The collector voltage is held at 0 V. The measurement is taken at the middle between two electrodes.

IV. Conclusions and Future work

In this work, we demonstrated our capability of kinetically modeling plasma in a chamber with novel quasi-neutral boundary conditions. The numerical results for the plasma sheath near a biased plate were validated against the analytical planar sheath model and the Bohm sheath criteria. With our high-fidelity kinetic PIC calculations, we showed that when a quick linear pulse with $\tau_{\text{electrons}} < \tau_{\text{pulse}} < \tau_{\text{ions}}$ is applied to a surface immersed in a quasineutral plasma, the electrons oscillate in at nearly all the locations in plasma. While the time-scales for the oscillations were found to be consistent with the variation of electron potential at various probe locations, we will employ plasma waves theory to understand the mechanism of these waves in future work.

We have also made progress in developing a multipole plasma chamber in UIUC Electric Propulsion Lab and have been successful in obtaining plasma similar to Langendorf et al.[5] In future work, we plan to validate our findings from the kinetic simulations against the plasma experiments with similar conditions.

Acknowledgement

This work is supported by the Air Force Office of Scientific Research through Grant AF FA9550-19-1-0164. This work (and Toyofumi Yamauchi) is supported in part by the Department of Education through the Graduate Assistance in Areas of National Need Fellowship Program award P200A180050-19 at the University of Illinois Urbana-Champaign Department of Aerospace Engineering.

References

[1]Ruzic, D. N., *Electric probes for low temperature plasmas*, American Vacuum Society, New York City, 1994.

[2]Jambunathan, R. and Levin, D. A., "Advanced parallelization strategies using hybrid MPI-CUDA octree DSMC method for modeling flow through porous media," *Computers & Fluids*, Vol. 149, 2017, pp. 70–87.

[3]Hershkowitz, N., "Sheaths: More complicated than you think," *Physics of plasmas*, Vol. 12, No. 5, 2005, pp. 055502.

[4]Jambunathan, R. and Levin, D. A., "CHAOS: An octree-based PIC-DSMC code for modeling of electron kinetic properties in a plasma plume using MPI-CUDA parallelization," *Journal of Computational Physics*, Vol. 373, 2018, pp. 571–604.

[5]Langendorf, S. and Walker, M., "Effect of secondary electron emission on the plasma sheath," *Physics of Plasmas*, Vol. 22, No. 3, 2015, pp. 033515.

[6]Nuwal, N. and Levin, D. A., "Numerical modeling of plasma-surface interactions in space vacuum," *AIAA Scitech 2020 Forum*, 2020, p. 2153.

[7]Riemann, K.-U., "The Bohm criterion and sheath formation," *Journal of Physics D: Applied Physics*, Vol. 24, No. 4, 1991, pp. 493.

[8]Johnson, J. and Holmes, A., "Edge effect correction for small planar Langmuir probes," *Review of scientific instruments*, Vol. 61, No. 10, 1990, pp. 2628–2631.

[9]Bradley, M. P. and Steenkamp, C. J., "Time-resolved ion and electron current measurements in pulsed plasma sheaths," *IEEE transactions on plasma science*, Vol. 34, No. 4, 2006, pp. 1156–1159.

[10]Hala, A. M. and Hershkowitz, N., "Ion acoustic wave velocity measurement of the concentration of two ion species in a multi-dipole plasma," *Review of Scientific Instruments*, Vol. 72, No. 5, May 2001, pp. 2279–2281.

[11]Langendorf, S. and Walker, M., "Effect of secondary electron emission on the plasma sheath," *Physics of Plasmas*, Vol. 22, No. 3, 2015, pp. 033515.

[12]Leung, K., Samec, T., and Lamm, A., "Optimization of permanent magnet plasma confinement," *Physics Letters A*, Vol. 51, No. 8, May 1975, pp. 490–492.

[13]Hershkowitz, N., DeKock, J. R., Coakley, P., and Cartier, S. L., "Surface trapping of primary electrons by multidipole magnetic fields," *Review of Scientific Instruments*, Vol. 51, No. 1, Jan. 1980, pp. 64–69.

[14]Arumugam, S., Alex, P., and Sinha, S. K., "Effective secondary electron emission coefficient in DC abnormal glow discharge plasmas," *Physics of Plasmas*, Vol. 24, No. 11, Nov. 2017, pp. 112106.

[15]Phelps, A. V. and Petrovic, Z. L., "Cold-cathode discharges and breakdown in argon: surface and gas phase production of secondary electrons," *Plasma Sources Science and Technology*, Vol. 8, No. 3, Aug. 1999, pp. R21–R44.